

DETECTION OF INTERSTELLAR ACETONE TOWARD THE ORION-KL HOT CORE

D. N. Friedel¹, L. E. Snyder¹, Anthony J. Remijan^{1,2,3}, and B. E. Turner⁴

ABSTRACT

We present the first detection of interstellar acetone $[(\text{CH}_3)_2\text{CO}]$ toward the high mass star forming region Orion-KL and the first detection of vibrationally excited $(\text{CH}_3)_2\text{CO}$ in the ISM. Using the BIMA Array, 28 emission features that can be assigned to 54 acetone transitions were detected. Furthermore, 37 of these transitions have not been previously observed in the ISM. The observations also show that the acetone emission is concentrated toward the hot core region of Orion-KL, contrary to the distribution of other large oxygen bearing molecules. From our rotational-temperature diagram we find a beam averaged $(\text{CH}_3)_2\text{CO}$ column density of $(2.0(0.3) - 8.0(1.2)) \times 10^{16} \text{ cm}^{-2}$ and a rotational temperature of 176(48)-194(66) K.

Subject headings: ISM:individual(Orion-KL)—ISM:molecules—radio lines:ISM

The first detection of interstellar acetone $[(\text{CH}_3)_2\text{CO}]$ was reported by Combes et al. (1987) and later confirmed by Snyder et al. (2002) towards the hot molecular core source Sgr B2(N-LMH). Previous to this paper, acetone had yet to be reported in any other high mass or low mass star forming region despite being structurally similar to dimethyl ether $((\text{CH}_3)_2\text{O})$. Conversely, $(\text{CH}_3)_2\text{O}$ has been detected in both low mass star forming regions including IRAS 16293-2422 (Cazaux et al. 2003) and high mass star forming regions including Sgr (Winnewisser & Gardner 1976) and Orion (Snyder et al. 1974). It seemed therefore likely that acetone may be prevalent in other star forming regions such as Orion-KL.

¹Department of Astronomy, 1002 W. Green St., University of Illinois, Urbana IL 61801
email: friedel@astro.uiuc.edu, snyder@astro.uiuc.edu

²NASA Goddard Space Flight Center, Computational and Information Sciences and Technologies Office, Code 606, Greenbelt, MD 20771
email: aremijan@pop900.gsfc.nasa.gov

³National Research Council Resident Research Associate

⁴National Radio Astronomy Observatory, Charlottesville, VA 22903
email: bturner@nrao.edu

The Orion-KL region is the closest (~ 480 pc) site of massive star formation (Genzel et al. 1981). There are several cloud components (e.g. hot core, compact ridge, extended ridge, and plateau) which are associated with Orion-KL, each with different chemical and physical properties (e.g. Blake et al. 1987). The two most chemically interesting components, the hot core and compact ridge, are separated by only ~ 5800 AU. Large oxygen bearing species (such as methyl formate (HCOOCH_3), dimethyl ether ($(\text{CH}_3)_2\text{O}$), and formic acid (HCOOH)) are observed primarily toward the compact ridge (e.g. Liu et al. 2002), while large nitrogen bearing species (i.e. vinyl cyanide ($\text{C}_2\text{H}_3\text{CN}$) and ethyl cyanide ($\text{C}_2\text{H}_5\text{CN}$)) are located toward the hot core (e.g. Blake et al. 1987).

In this letter, we present the first detection of interstellar $(\text{CH}_3)_2\text{CO}$ toward the high mass star forming region Orion-KL and the first detection of vibrationally excited $(\text{CH}_3)_2\text{CO}$ in the ISM. Using the Berkeley-Illinois-Maryland Association (BIMA)¹ Array, 28 emission features that can be assigned to 54 acetone transitions were detected toward the Orion hot core. The detection of $(\text{CH}_3)_2\text{CO}$ toward the Orion hot core is unusual since it is a complex oxygen bearing species, structurally similar to $(\text{CH}_3)_2\text{O}$, a compact ridge species. This indicates that the formation of $(\text{CH}_3)_2\text{CO}$ may be very different than $(\text{CH}_3)_2\text{O}$ and may invoke N bearing species or grain surface reactions. Finally, since acetone is prevalent toward the Orion hot core region, it is most likely that a spectral line assigned as interstellar glycine ($\text{NH}_2\text{CH}_2\text{COOH}$) toward the Orion-KL region can be assigned instead to interstellar $(\text{CH}_3)_2\text{CO}$.

The data presented were taken between 2002 and 2003 November as part of a 3mm spectral line survey of the Orion-KL region by the BIMA Array (Friedel et al., 2006 in prep.) in its C configuration. The phase center of our observations was $\alpha(\text{J2000})=05^{\text{h}}35^{\text{m}}4^{\text{s}}.3$, $\delta(\text{J2000})=-05^{\circ}22'27''.6$, which is near the hot core ($\alpha(\text{J2000})=05^{\text{h}}35^{\text{m}}14^{\text{s}}.5$, $\delta(\text{J2000})=-5^{\circ}22'30''$) and the compact ridge ($\alpha(\text{J2000})=05^{\text{h}}35^{\text{m}}14^{\text{s}}.2$, $\delta(\text{J2000})=-5^{\circ}22'41''$). The array was operating in cross-correlation (double-sideband) mode with a sideband rejection of better than 20 dB. The correlator was configured to have four 50 MHz wide windows in each sideband with 128 channels per window. This resulted in a channel spacing of 391 kHz ($\sim 1.4 - 1.1$ km s^{-1}), for all observations. Saturn was used as the flux density calibrator and 0423-013 and 0609-157 were used to calibrate the antenna based gains. The absolute amplitude calibration of 0423-013 and 0609-157 from the flux density calibrators is accurate to within $\sim 20\%$. The passbands were automatically calibrated during data acquisition. The data were calibrated, continuum subtracted and imaged using the MIRIAD software package (Sault et al. 1995). The ground state $(\text{CH}_3)_2\text{CO}$ molecular parameters were taken from Groner et al. (2002) and

¹Operated by the University of California, Berkeley, the University of Illinois, and the University of Maryland with support from the National Science Foundation.

the vibrational $(\text{CH}_3)_2\text{CO}$ molecular parameters were taken from Groner et al. (2005).

Table 1 lists the molecular parameters and observational results for the detected acetone lines. Column 1 lists the rest frequency in MHz, column 2 lists the quantum numbers, column 3 lists the upper state energy (E_u) in K, column 4 lists the line strength (S_{ij}), column 5 lists the spin weight, column 6 lists the integrated line intensity (W) in $\text{Jy beam}^{-1} \text{ km s}^{-1}$, column 7 lists the rest velocity of the transitions (V_{LSR}) in km s^{-1} , column 8 lists the synthesized beam size in arcseconds, and column 9 lists the figure in which the associated spectra appear. We detected a total of 28 spectral features that can be assigned to 54 $(\text{CH}_3)_2\text{CO}$ transitions, 37 of which have not been previously observed in the ISM, toward the Orion hot core. Of these 54 transitions 46 are from the ground state and 8 are from the first vibrationally excited state which lies at 115 K above ground. No $(\text{CH}_3)_2\text{CO}$ transitions were seen, above our 3σ limit, toward the Orion compact ridge.

Figure 1 shows the spectra of each of our detected transitions and nearby identified and unidentified lines. All spectra are hanning smoothed over 3 channels and the spectral line fiducials are for a V_{LSR} of 5 km s^{-1} . The “I” bar in the upper left corner of each plot denotes the 1σ rms noise level for the plot. In subplots c) and d) the dashed line and second “I” bar denote where a second spectral window was located and the associated 1σ rms noise level of that window.

Figure 2 shows the map of the $8_{*,8} - 7_{*,7} EE$ degenerate transitions of $(\text{CH}_3)_2\text{CO}$ ($E_u=19$ K) in heavy contours. Contours are ± 3 and 5σ ($\sigma=0.09 \text{ Jy beam}^{-1}$). The normal contours are the $7_{0,7} - 6_{1,6}$ four fold degenerate transition of $(\text{CH}_3)_2\text{O}$ ($E_u=25$ K, $\nu=111.783112$ GHz). Contour spacing is 4σ starting at 4σ ($\sigma=0.24 \text{ Jy beam}^{-1}$). The hot core and compact ridge are labeled and indicated by the “+” signs. Note that the $(\text{CH}_3)_2\text{CO}$ emission traces closer to the hot core while the $(\text{CH}_3)_2\text{O}$ emission traces closer to the compact ridge. The synthesized beams for each species are in the lower left corner of the map. The average V_{LSR} for the detected $(\text{CH}_3)_2\text{CO}$ transitions is $6.4(1.3)^2 \text{ km s}^{-1}$ which is between the V_{LSR} for the hot core ($\sim 5 \text{ km s}^{-1}$) and the compact ridge ($\sim 8 \text{ km s}^{-1}$). Yet it is consistent with the V_{LSR} of other molecular species (Blake et al. 1987). The maps of the transitions, however, indicate that $(\text{CH}_3)_2\text{CO}$ is more closely associated with the hot core rather than the compact ridge (Blake et al. 1987).

For interferometric observations the total column density $\langle N_T \rangle$ can be calculated from (Snyder et al. 2002, 2005):

$$\frac{\langle N_T \rangle}{q_{rv}} e^{-E_u/T_{rot}} = \frac{\langle N_u \rangle}{g_u} = \frac{2.04}{B\theta_a\theta_b S\mu^2\nu^3} \left(\frac{W}{g} \right) \times 10^{20} \text{ cm}^{-2} \quad (1)$$

²All uncertainties are 1σ unless otherwise noted.

where $\langle N_u \rangle / g_u$ is the beam averaged upper level column density over the statistical weight, B is the beam filling factor, g is the spin weight, μ is the dipole moment ($\mu_b = 2.93$ D), ν is the transition frequency in GHz, T_{rot} is the rotational temperature and E_u is the upper level energy of the transition in K. The rotational-vibrational partition function, q_{rv} , is defined as

$$q_{rv} \approx \sum_{i=0}^2 e^{-E_i/T_{rot}} q_r, \quad (2)$$

where E_i are the energies above ground for the ground state and the first two vibrational states (0 K, 115 K, and 180 K, respectively) and q_r is the rotational partition function³ ($261.7T_{rot}^{3/2}$) (Groner et al. 2002, 2005; Widicus Weaver et al. 2005). Even though we did not detect any transitions from the second vibrationally excited state, it lies only 180 K above ground and thus will have a significant population at temperatures above 100 K. For a set of degenerate transitions, g is the sum of the spin weights of the blended states. By plotting $\ln(\langle N_u \rangle / g_u)$, for each integrated line intensity in Table 1, versus E_u we can obtain the total beam averaged column density and rotational temperature of $(\text{CH}_3)_2\text{CO}$. Figure 3 shows the rotational-temperature diagram (assuming the source fills our synthesized beams, $B = 0.5$, as discussed by Snyder et al. (2005)) and yields $\langle N_T \rangle = 2.0(0.3) \times 10^{16} \text{ cm}^{-2}$ and $T_{rot} = 176(48)$ K. If instead we assume a source size similar to the hot core continuum size seen by Liu et al. (2002) of $5'' \times 3''$, the diagram yields $\langle N_T \rangle = 8.0(1.2) \times 10^{16} \text{ cm}^{-2}$ and $T_{rot} = 194(66)$ K. Both temperatures are reasonable considering the range in temperatures observed toward the hot core (~ 100 K ($\text{C}_2\text{H}_5\text{CN}$, White et al. 2003) to ~ 300 K (HC_3N , Wright et al. 1996)). From these column densities, rotation temperatures, and Turner (1991) we calculated the opacity to be < 0.02 for all transitions. For a H_2 column density of $\sim 5 \times 10^{24} \text{ cm}^{-2}$ (Kaufman et al. 1998, and references therein) we find a fractional abundance of $(4.0(0.6) - 16.0(2.4)) \times 10^{-9}$ which is higher than the fractional abundance of $(\text{CH}_3)_2\text{CO}$ toward Sgr B2(N-LMH) ($4 - 30 \times 10^{-10}$) (Snyder et al. 2002). The difference however can be attributed our use of the vibrational part of the partition function. If we recalculate the abundances from Sgr B2(N-LMH) including the vibrational part of the partition function it agrees with our abundance toward Orion.

The detection of $(\text{CH}_3)_2\text{CO}$ toward the hot core and the non-detection (above 3σ) toward the compact ridge, makes $(\text{CH}_3)_2\text{CO}$ the only known highly saturated O species that is seen only toward the hot core. This suggests a formation mechanism such as high temperature gas phase reactions (i.e. neutral-neutral) or grain surface reactions, as was

³The rotational part of the partition function is approximated by the ground state q_r since q_r for the first vibrational state differs from the ground state by less than 1 part in 1000 and q_r for the second vibrational state has not been reported.

suggested by Herbst et al. (1990), rather than formation in or behind a shock front (i.e. ion-molecule chemistry or liberation from the grain surface).

Finally, the detection of acetone toward the Orion hot core is also very significant because it shows that a spectral feature previously identified as glycine may in fact be due to interstellar acetone. Kuan et al. (2003) noted that one of the lines assigned to glycine was coincident with the $31_{*,19} - 31_{*,20} EE$ degenerate $(\text{CH}_3)_2\text{CO}$ pair. The identification of a transition of $(\text{CH}_3)_2\text{CO}$ was dismissed as unlikely due to its unfavorable quantum numbers. However, we can calculate the expected integrated intensity for these degenerate acetone transitions using the $(\text{CH}_3)_2\text{CO}$ column densities from this work and from eqs. [1] & [2] of Snyder et al. (2005). Solving eqs. [1] & [2] of Snyder et al. (2005) for the integrated line intensity (W) we find:

$$W = \frac{\langle N_T \rangle g S \mu^2 \nu B^*}{1.67 q_{rv} e^{E_u/T_{rot}}} \times 10^{-14} \text{ K km s}^{-1}, \quad (3)$$

where, for these transitions, $g = 16 + 16 = 32$, $S = 12.555$, $\nu = 164.870$ GHz, and $E_u = 364$ K. Also $B^* = \eta_M^* B$, where η_M^* is the corrected main beam efficiency for the 12 meter ($\eta_M^* \sim 0.7$ at 164 GHz). If we use the $5'' \times 3''$ source size and associated $\langle N_T \rangle$ and T_{rot} we calculate an integrated line intensity of $0.218(0.031)$ K km s⁻¹. Comparing this value to that reported by Kuan et al. (2003) of $0.091(0.035)$ K km s⁻¹ we see that the integrated line intensity overlaps with the reported value at the 2σ level. Because of the detection of 54 transitions of interstellar $(\text{CH}_3)_2\text{CO}$ toward the Orion hot core, it is most likely that the transition attributed to glycine by Kuan et al. (2003) is due to $(\text{CH}_3)_2\text{CO}$.

We have reported the detection of 54 $(\text{CH}_3)_2\text{CO}$ transitions toward the Orion-KL hot core region with a column density of $(2.0(0.3) - 8.0(1.2)) \times 10^{16}$ cm⁻² and a rotational temperature of $176(48)$ - $194(66)$ K. We also have reported the first detection of vibrationally excited $(\text{CH}_3)_2\text{CO}$ in the ISM. The detection of a large O bearing species purely toward the hot core suggests that the formation of $(\text{CH}_3)_2\text{CO}$ may be very different than $(\text{CH}_3)_2\text{O}$ and may invoke N bearing species or grain surface reactions.

We thank P. Groner and B. Drouin for supplying useful data. We also thank an anonymous referee for a very favorable review of this work. This work was partially funded by grant NSF AST02-28953 and the University of Illinois.

REFERENCES

- Blake, G. A., Sutton, E. C., Masson, C. R., & Phillips, T. G. 1987, *ApJ*, 315, 621
- Cazaux, S., Tielens, A. G. G. M., Ceccarelli, C., Castets, A., Wakelam, V., Caux, E., Parise, B., & Teyssier, D. 2003, *ApJ*, 593, L51
- Combes, F., Gerin, M., Wootten, A., Wlodarczak, G., Clausset, F., & Encrenaz, P. J. 1987, *A&A*, 180, L13
- Kuan, Y., Charnley, S. B., Huang, H., Tseng, W., & Kisiel, Z. 2003, *ApJ*, 593, 848
- Genzel, R., Reid, M. J., Moran, J. M., & Downes, D. 1981, *ApJ*, 244, 884
- Groner, P., Herbst, E., De Lucia, F. C., Drouin, B. J., & Mäder, H. 2005, 60th OSU International Conference on Molecular Spectroscopy, RA03, 206
- Groner, P., Albert, S., Herbst, E., De Lucia, F. C., Lovas, F. J., Drouin, B. J., & Pearson, J. C. 2002, *ApJS*, 142, 145
- Herbst, E., Giles, K., & Smith, D. 1990, *ApJ*, 358, 468
- Kaufman, M. J., Hollenbach, D. J., & Tielens, A. G. G. M. 1998, *ApJ*, 497, 276
- Liu, S., Girart, J. M., Remijan, A., & Snyder, L. E. 2002, *ApJ*, 576, 255
- Sault, R. J., Teuben, P. J., & Wright, M. C. H. 1995, *ASP Conf. Ser.* 77: *Astronomical Data Analysis Software and Systems IV*, 77, 433
- Schilke, P., Groesbeck, T. D., Blake, G. A., & Phillips, T. G. 1997, *ApJS*, 108, 301
- Snyder, L. E., Buhl, D., Schwartz, P. R., Clark, F. O., Johnson, D. R., Lovas, F. J., & Giguere, P. T. 1974, *ApJ*, 191, L79
- Snyder, L. E., Lovas, F. J., Mehringer, D. M., Miao, N. Y., Kuan, Y., Hollis, J. M., & Jewell, P. R. 2002, *ApJ*, 578, 245
- Snyder, L. E., et al. 2005, *ApJ*, 619, 914
- Turner, B. E. 1991, *ApJS*, 76, 617
- Ulich, B. L., & Haas, R. W. 1976, *ApJS*, 30, 247
- White, G. J., Araki, M., Greaves, J. S., Ohishi, M., & Higginbottom, N. S. 2003, *A&A*, 407, 589

Widicus Weaver, S. L., Butler, R. A. H., Drouin, B. J., Petkie, D. T., Dyl, K. A., De Lucia, F. C., & Blake, G. A. 2005, *ApJS*, 158, 188

Winnewisser, G., & Gardner, F. F. 1976, *A&A*, 48, 159

Wright, M. C. H., Plambeck, R. L., & Wilner, D. J. 1996, *ApJ*, 469, 216

Table 1. Acetone ((CH₃)₂CO) Molecular Line and Observational Parameters^a

Frequency (MHz) ^b	Quantum Numbers	E_u (K)	S_{ij}	Spin Wt.	W (Jy bm ⁻¹ km s ⁻¹)	V_{LSR} (km s ⁻¹)	$\theta_a \times \theta_b$ (")	Fig.
81,813.725 (12)	7 _{1,6} – 6 _{2,5} EE	17.47	5.21	16	1.5(1.0)	6.6(2.5)	12.99 × 8.33	^c
82,895.112 (52)	8 _{*,8} – 7 _{*,7} EE, $\nu = 1^{d,e}$	133.95	7.38	32	2.1(0.6)	6.0(2.3)	12.54 × 7.86	1a
82,908.654 (20)	8 _{*,8} – 7 _{*,7} AE	18.85	7.38	8	1.7(0.3)	6.9(0.9)	12.54 × 7.86	1a
82,908.702 (20)	8 _{*,8} – 7 _{*,7} EA	18.85	7.38	8	f			1a
82,916.525 (14)	8 _{*,8} – 7 _{*,7} EE	18.74	7.38	32	3.0(0.3)	7.3(0.4)	12.54 × 7.86	1a
82,924.325 (22)	8 _{*,8} – 7 _{*,7} AA	18.64	7.38	16	2.8(0.5)	7.5(1.1)	12.54 × 7.86	1a
87,507.547 (46)	18 _{8,10} – 18 _{7,11} EE ^{d,e}	130.60	8.27	16	2.8(0.3)	6.6(2.4)	13.16 × 9.21	1b
87,580.004 (44)	18 _{9,10} – 18 _{8,11} EE ^{d,e}	130.60	8.27	16	1.4(0.7)	4.5(0.5)	11.82 × 7.81	^c
92,714.466 (54)	9 _{*,9} – 8 _{*,8} EE, $\nu = 1^{d,e}$	138.41	8.38	32	3.1(0.8)	8.3(6.9)	13.89 × 6.20	1c
92,727.906 (22)	9 _{*,9} – 8 _{*,8} AE	23.30	8.38	8	3.3(0.9)	5.8(0.8)	13.89 × 6.20	1c
92,727.952 (20)	9 _{*,9} – 8 _{*,8} EA	23.30	8.38	8	f			1c
92,735.672 (16)	9 _{*,9} – 8 _{*,8} EE	23.19	8.38	32	4.1(0.5)	6.9(1.9)	13.89 × 6.20	1c
92,743.363 (24)	9 _{*,9} – 8 _{*,8} AA	23.09	8.38	16	g			1c
93,311.552 (90)	22 _{12,11} – 22 _{11,12} EE ^{d,e}	198.48	11.29	16	1.8(0.7)	6.5(1.7)	14.86 × 6.91	1d
98.651.514 (20)	5 _{5,1} – 4 _{4,1} EE ^{d,e}	14.09	3.63	16	5.6(0.4)	7.0(3.0)	13.86 × 6.19	1e
98,800.980 (14)	5 _{5,0} – 4 _{4,0} EE ^{d,e}	14.09	3.63	16	3.7(0.3)	6.2(1.3)	15.54 × 7.03	1f
99,422.080 (24)	14 _{*,11} – 14 _{*,12} EE ^{d,e}	68.11	3.33	32	2.7(0.5)	4.7(2.1)	13.64 × 6.61	1g
101,426.716 (19)	9 _{1,8} – 8 _{2,7} AE/EA ^d	26.84	7.21	10	4.7(0.4)	6.3(0.5)	12.91 × 6.74	1h
101,427.090 (19)	9 _{2,8} – 8 _{1,7} AE/EA ^d	26.84	7.21	6	f			1h
101,451.059 (14)	9 _{1,8} – 8 _{2,7} EE ^d	26.74	7.21	16	7.2(0.3)	6.7(1.0)	13.35 × 6.94	1h
101,451.446 (14)	9 _{2,8} – 8 _{1,7} EE ^d	26.74	7.21	16	f			1h
101,475.332 (22)	9 _{1,8} – 8 _{2,7} AA ^d	26.64	7.21	10	h			1h
101,475.733 (22)	9 _{2,8} – 8 _{1,7} AA ^d	26.64	7.21	6	h			1h
102,533.756 (58)	10 _{*,10} – 9 _{*,9} EE, $\nu = 1^{d,e,i}$	143.33	9.37	32	2.7(0.5)	6.3(1.5)	12.80 × 6.17	1i
102,547.058 (22)	10 _{0,10} – 9 _{1,9} AE/EA ^d	28.22	9.38	16	j			1i
102,554.696 (18)	10 _{0,10} – 9 _{1,9} EE ^d	28.11	9.38	32	4.5(0.4)	6.9(1.9)	12.80 × 6.17	1i
102,562.281 (26)	10 _{0,10} – 9 _{1,9} AA ^d	28.01	9.38	16	4.7(0.5)	6.8(2.4)	12.80 × 6.17	1i
108,434.511 (32)	14 _{2,12} – 14 _{1,13} EE ^{d,e}	63.34	2.29	32	2.0(0.5)	6.9(1.1)	12.22 × 5.64	1j
111,243.359 (22)	10 _{*,9} – 9 _{*,8} AE ^d	32.17	8.21	8	3.6(0.4)	7.1(1.2)	12.44 × 5.77	1k
111,243.448 (20)	10 _{*,9} – 9 _{*,8} EA ^d	32.17	8.21	8	f			1k
111,267.540 (16)	10 _{*,9} – 9 _{*,8} EE ^d	32.07	8.21	32	5.6(0.2)	6.6(0.9)	12.44 × 5.77	1k
111,291.600 (24)	10 _{*,9} – 9 _{*,8} AA ^d	31.98	8.21	16	k			1k
112,352.908 (60)	11 _{*,11} – 10 _{*,10} EE, $\nu = 1^{d,e}$	148.71	10.37	32	l			1l
112,373.548 (18)	11 _{0,11} – 10 _{1,10} EE ^{d,e}	33.51	10.39	32	m			1l

^aDegenerate pairs of transitions are denoted with a * in the quantum numbers or list two torsional states (i.e. AE/EA). The reported frequency is the average frequency of the transitions and the reported spin weight is the sum from the transitions. See Groner et al. (2002) and Groner et al. (2005) for a complete listing.

^bFrequency uncertainty is 2σ .

^cThis transition will be shown in Friedel et al. (2006, in prep.).

^dNot previously observed in ISM.

^eThe AA, AE and EA transitions were below the 3σ detection limit.

^fThis transition is blended with the previous one(s) and the integrated line intensity and column density are calculated as such.

^gThe AA transitions are less than 3σ and thus are not used in the calculations.

^hThis transition is blended with the $18_{3,15} - 18_{3,16}E$ transition of methyl formate (HCOOCH_3).

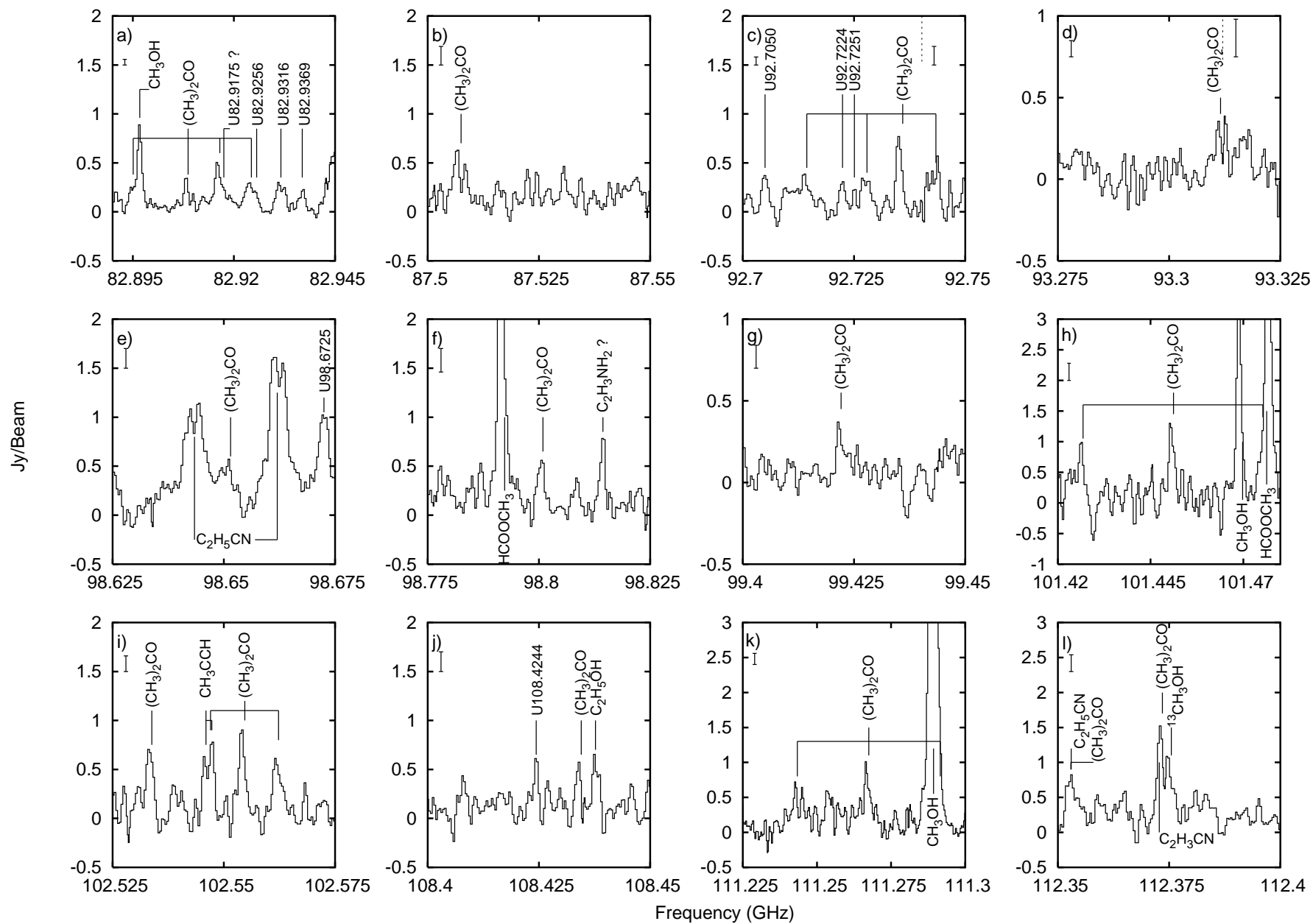
ⁱThis transition of $(\text{CH}_3)_2\text{CO}$ is coincident with the $6_{0,6} - 5_{0,5}$ transition of ethanol ($\text{C}_2\text{H}_5\text{OH}$), however since $\text{C}_2\text{H}_5\text{OH}$ is thought to be a compact ridge species (Schilke et al. 1997) and is only weakly detected toward the compact ridge, we consider the contamination from $\text{C}_2\text{H}_5\text{OH}$ to be minimal.

^jThis transition is blended with the $6_0 - 5_0$ transition of propyne (CH_3CCH).

^kThis transition is blended with the $7_{2,5} - 8_{1,8}A+$ transition of methanol (CH_3OH).

^lThis transition is blended with the $11_{1,11} - 10_{0,10}A \nu_t = 1$ transition of ethyl cyanide ($\text{C}_2\text{H}_5\text{CN}$).

^mThis transition may be blended with the $8_{1,8} - 7_{0,7} \ ^1\nu_{11}$ transition of vinyl cyanide ($\text{C}_2\text{H}_3\text{CN}$) and is not used in the calculations.



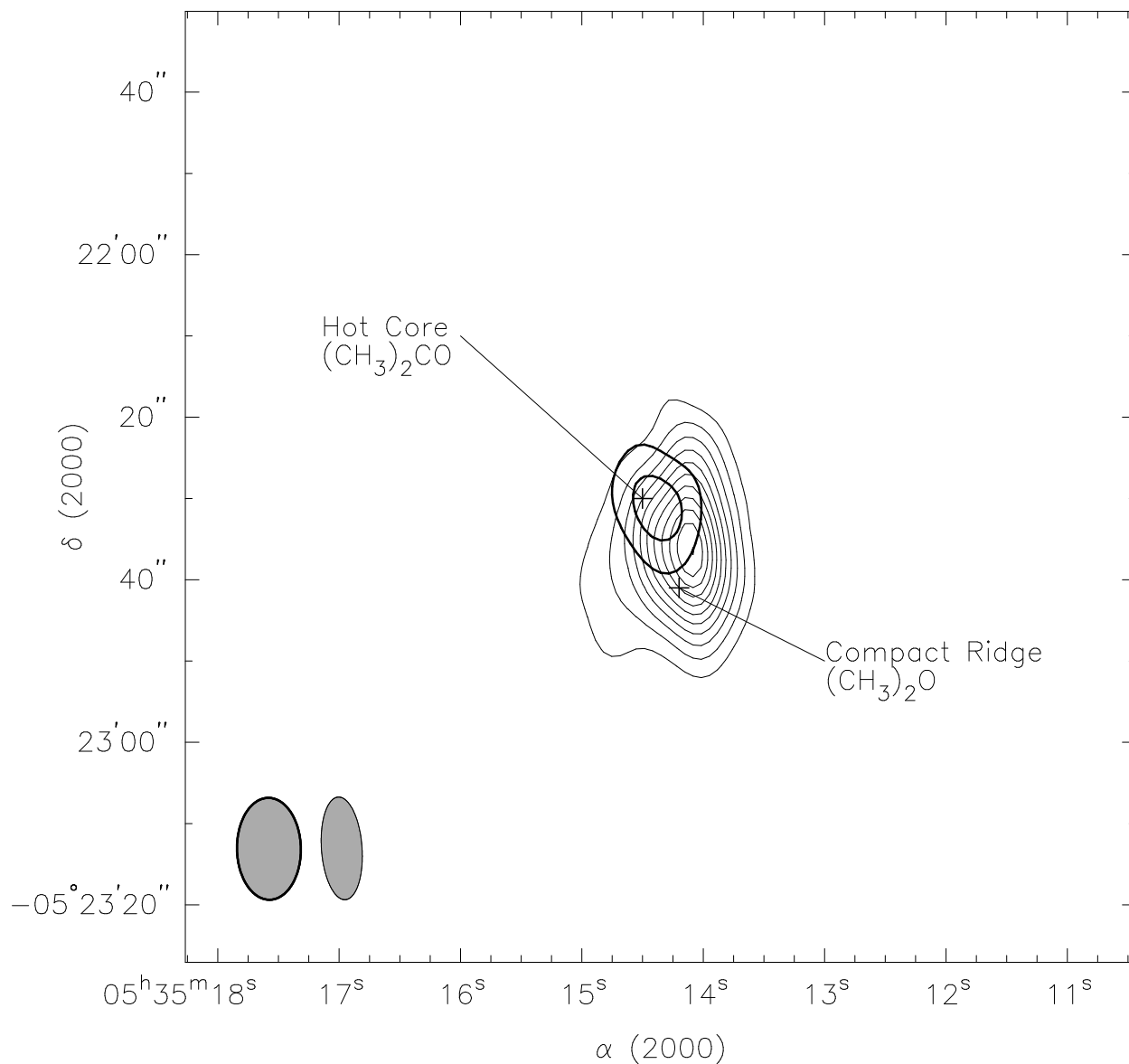


Fig. 2.— Contour maps of acetone and dimethyl ether toward the Orion KL region. Heavy contours are the $8_{*,8} - 7_{*,7}EE$ degenerate transitions of $(\text{CH}_3)_2\text{CO}$ ($E_u=19$ K). Contour levels are $\pm 3, 5 \sigma$ ($\sigma = 0.09$ Jy beam $^{-1}$). The normal contours are the $7_{0,7} - 6_{1,6}$ degenerate transitions of $(\text{CH}_3)_2\text{O}$ ($E_u=25$ K, $\nu=111.783112$ GHz). Contour spacings are 4σ starting at 4σ ($\sigma = 0.24$ Jy beam $^{-1}$). The hot core and compact ridge are labeled with “+”. The synthesized beams for the respective maps are in the lower left corner.

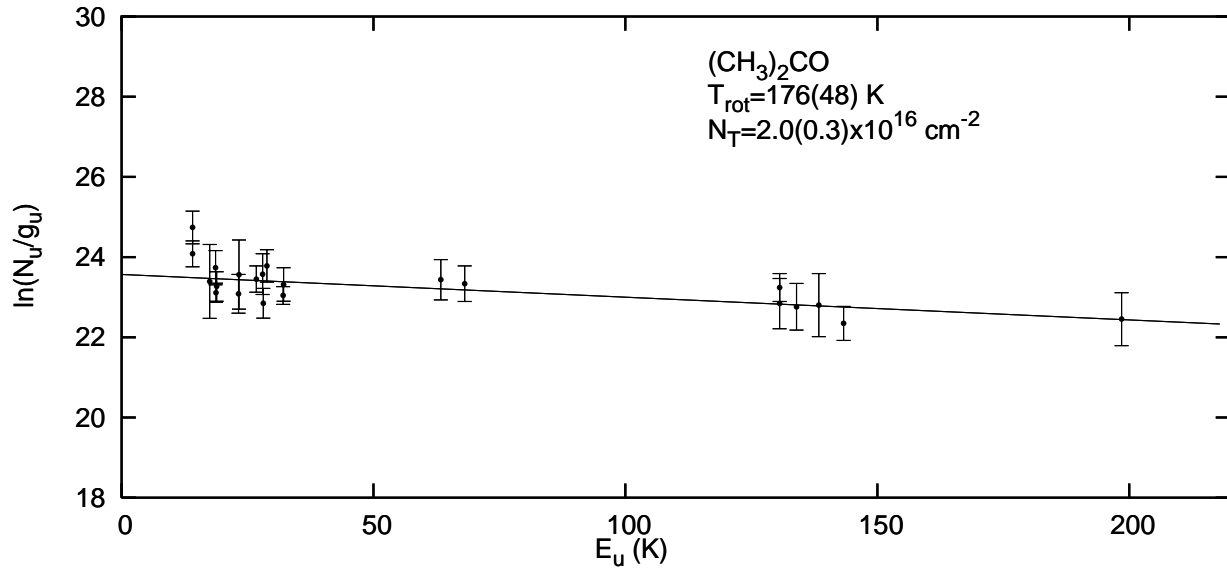


Fig. 3.— Rotational temperature diagram for detected acetone transitions. The ordinate is $\ln(\langle N_u \rangle / g_u)$, the abscissa is E_u in K, and the uncertainties are 1σ . The weighted least squares fit is shown by the line. The resulting rotational temperature and column density are shown.